



HAL
open science

Silicon carbide PIN diode for tritium detection

Paul Eyméoud, Stéphane Biondo, Vanessa Vervisch, Laurent Ottaviani, Nadia Grillet, Luc Roussel, Karine Coulié, Olivier Palais, Julien Darréon, Wilfried Vervisch

► **To cite this version:**

Paul Eyméoud, Stéphane Biondo, Vanessa Vervisch, Laurent Ottaviani, Nadia Grillet, et al.. Silicon carbide PIN diode for tritium detection. 2025. hal-04906557

HAL Id: hal-04906557

<https://amu.hal.science/hal-04906557v1>

Preprint submitted on 22 Jan 2025

HAL is a multi-disciplinary open access archive for the deposit and dissemination of scientific research documents, whether they are published or not. The documents may come from teaching and research institutions in France or abroad, or from public or private research centers.

L'archive ouverte pluridisciplinaire **HAL**, est destinée au dépôt et à la diffusion de documents scientifiques de niveau recherche, publiés ou non, émanant des établissements d'enseignement et de recherche français ou étrangers, des laboratoires publics ou privés.

Silicon carbide PIN diode for tritium detection

Paul Eyméoud^{a,*}, Stéphane Biondo^b, Vanessa Vervisch^a, Laurent Ottaviani^c, Nadia Grillet^c,
Luc Roussel^c, Karine Coulié^c, Olivier Palais^c, Julien Darréon^d and Wilfried Vervisch^{a,c}

^a*SiClade Technologies, 2013 Chemin des Ratonneaux, 13680 Lançon-Provence, France*

^b*Magdala, 1641 RN8, 13400 Aubagne, France*

^c*Aix-Marseille Univ., Université de Toulon, CNRS, IM2NP, Marseille, France*

^d*Institut Paoli-Calmettes, Marseille, France*

ARTICLE INFO

Keywords:

Tritium detection

Silicon carbide

PIN diode

Numerical simulation

ABSTRACT

We have designed a prototype of silicon carbide PIN diode for tritium detection. Monte-Carlo calculations showed the necessity to work in vacuum and employ thin and low-density coating layers, and drew the energy deposition profile in the device. The deposited energies have then been used to implement finite-elements simulations, in order to optimize three structural parameters (n -doping concentration, p doping concentration, p zone thickness) maximizing the electrical response. Temperature lowering improves the diode electrical response.


In nuclear industry, tritium is the key reactant for ITER world fusion program, and a secondary waste from Canadian Pressurized Heavy-Water Reactors CANDU. Because of its volatility in air and water, and ecotoxicity, quantification of tritium environmental rejections represents an important nuclear safety topic [1]. Among the numerous available tritium detection approaches [2, 3], the beta-voltaic detection presents several advantages: simple to implement and non-destructive, it offers a real-time lecture of tritium dosimetry. It consists in collecting the electrons produced from tritium β^- decay in a diode that will produce an electrical signal [4]. Nevertheless, the main technological challenge of this beta-voltaic approach is the necessity to get a diode sensitive enough to detect very low energy electrons (maximum and average energy of 18.5 and 5.7 keV, respectively) with a low dose rate (around 1 electron per second, inducing very low signal-to-noise ratio). To reach that goal, the use of large bandgap semiconductors allows to significantly increase detection efficiency [5], compared to usual low bandgap devices previously implemented with Si [4, 6, 7, 8], GaAs [9] or InGaP [10]. Among the standard wide bandgap semiconductors employed to design a diode, we will privilege silicon carbide (SiC), currently cheaper and larger in surface detection dimension, than diamond and gallium nitride.

This communication, divided into two parts, recaps the development of a SiC-based PIN diode for tritium detection. First, we have performed Monte-Carlo calculations using MCNP code [11], in order to investigate the screening effect of ambient atmosphere and diode coatings with respect to the electrons produced from tritium decay, and evaluate the energy deposited by these electrons in the diode. Second, we have realized finite elements simulations with Sentauros code [12], in order to draw an optimal design for the diode, maximizing its electrical response.

The Monte-Carlo calculations have been performed with MCNP code using p,e mode, with $nps = 10^8$ sources particles histories, in order to get a better precision than anterior studies realized at $nps = 4 \cdot 10^6$ [13] and $nps = 2.4 \cdot 10^7$ [14]. We have represented in a simulation box containing vacuum (see Fig. 1a) a layer of studied material, which is bombarded by a monodirectional disk source mimicking tritium beta decay spectrum, fitted from 54 points on the data from [15]. The resulting electron spectrum has given good correlation with the Fermi statistics from Ref. [16] (see Supplementary Material).

We have first focused on the case of screening effect of ambient atmosphere (dry air at sea level altitude, density fixed to $0.001205 \text{ g} \cdot \text{cm}^{-3}$), by counting the electrons moving through the air sample. In a previous work [13] we found a factor 5.7 screening effect (resp. quasi-total screening effect) after 1 mm of air (resp. 5 mm of air) at 1 bar. Here, we have implemented two vacuum conditions, 0.1 bar and 0.01 bar, in order to evaluate how the pressure chamber affects the screening effect of air (cf. Figure 1b). The averaging on complete spectra, detailed in Table 1, revealed than one can reasonably work experimentally under 0.1 bar pressure condition, with a 1 cm distance between diode and sample, that leads to less than 60% screening effect.

*Corresponding author.

 paul.eymeoud@siclade-technologies.com (P. Eyméoud)
ORCID(s): 0000-0003-4705-4244 (P. Eyméoud)

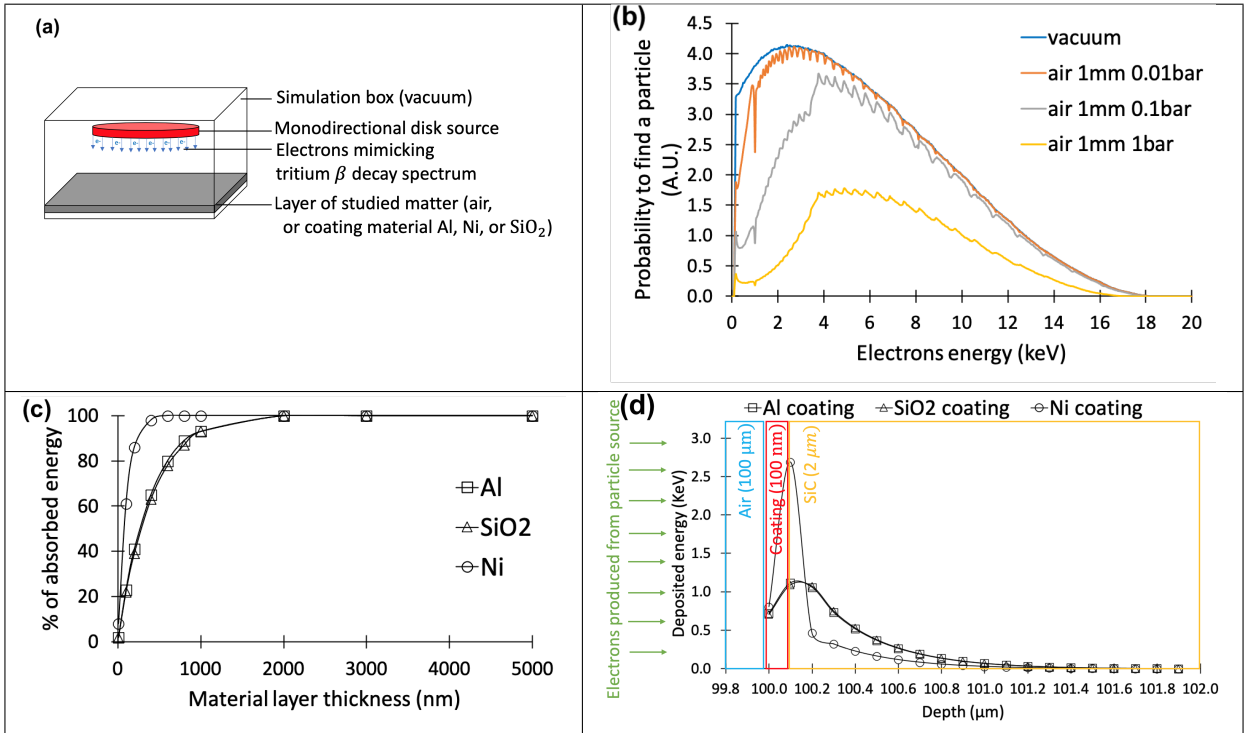


Figure 1: Monte-Carlo calculations: (a) structure of MCNP screening effect simulation, (b) screening effect of air, and consequence of pressure lowering in measuring chamber (spectra), (c) screening effect of coating materials (absorbed energy), (d) deposition energy profile in diode for three different coatings. Calculation uncertainties are given in Supplementary Material.

Table 1

Screening effect of air: absorbed energy of electrons (%), as function of air layer parameters (thickness and pressure).

Air layer thickness	1 mm	5 mm	10 mm
Air pressure 1 bar	55%	99%	99.9%
Air pressure 0.1 bar	10%	35%	55.3%
Air pressure 0.01 bar	1%	5.5%	10%

In a second step, we have focus on the case of the screening effect of three coating candidate materials for the diode (cf. Fig. 1c), showing a quasi-equivalent screening effect for Al and SiO₂ coatings (because of their similar densities), becoming quasi-total after 2 μ m of material, and a higher screening effect for Ni coating, becoming quasi-total after 0.5 μ m of material. Finally, a realistic simulation of energy deposition in diode (described on Fig. 1d: tritium source + air medium at 1 bar + 100 nm coating layer + SiC detection material) has been performed for the three coating materials (Al, SiO₂ and Ni). The Ni-coated diode appears to be unfavorable (majority of the deposition realized in the coating), contrary to the Al- and SiO₂-coated diodes (moderate deposition in the coating, followed by a clean deposition in the first micrometer of SiC). We have concluded that, for an optimal detection, it was necessary to employ thin coating layers of low-density materials such as Al or SiO₂, in coherence with [13], and to use the upstream surface part of SiC.

The energy depositions obtained for the Al-coated diode have been used to estimate an electron-hole generation rate in an SiC-based diode with Al coating, through the following equation:

$$\tau = \frac{\langle E \rangle \cdot D}{C_r \cdot V_{\text{active}}}$$

wherein τ denotes the generation rate (in (number of e/h pairs) \cdot cm⁻³ \cdot s⁻¹), $\langle E \rangle$ the average deposited energy computed with MCNP, D the number of disintegrations (in Bq), V_{active} the active zone volume (in cm³), and C_r the

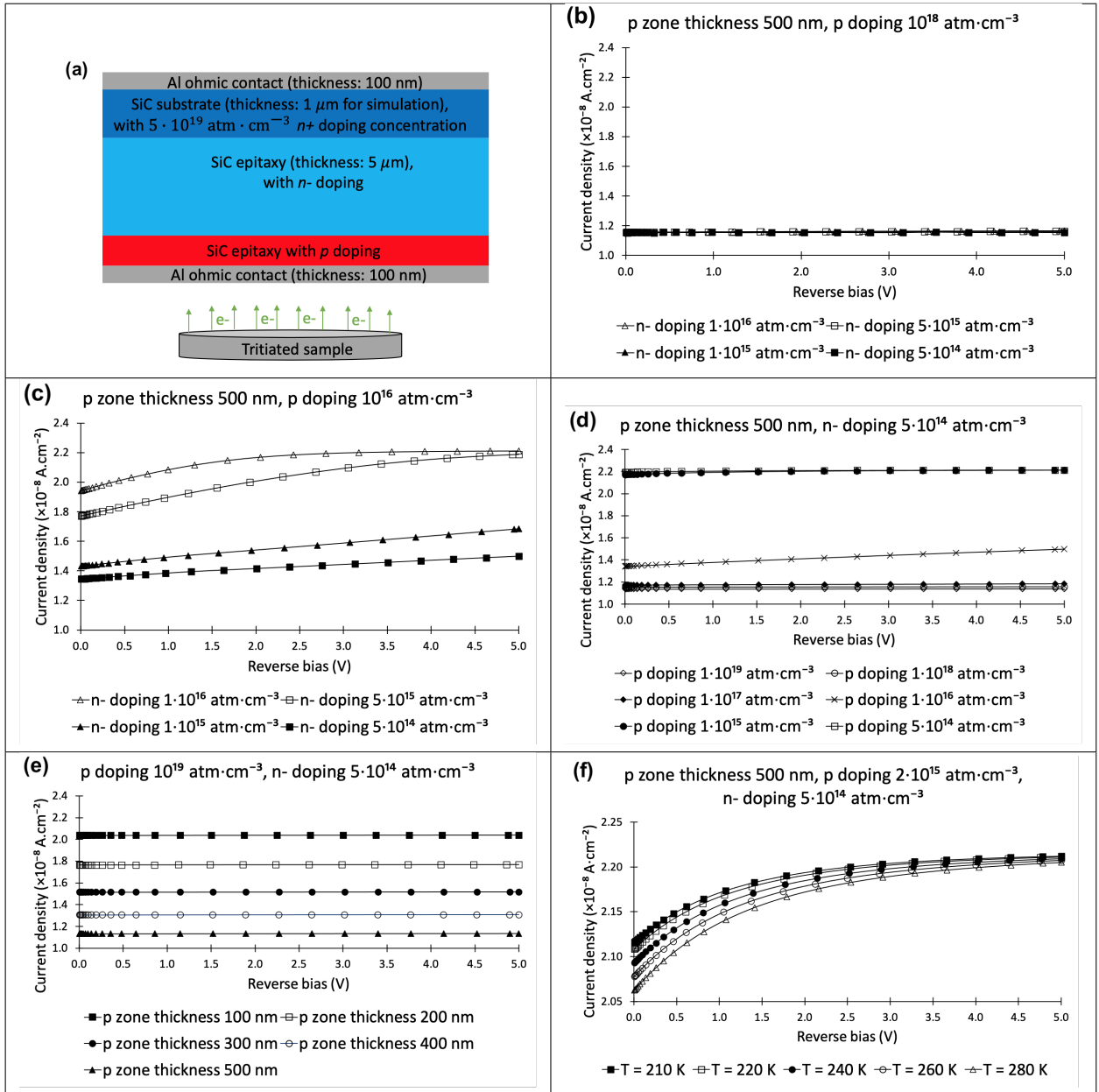


Figure 2: Finite elements calculations: (a) structure of Sentaurus simulation (three varying parameters: p zone thickness, doping concentration in p zone, doping concentration in n -zone), (b) impact of n -doping concentration on electrical response for high p doping concentration, (c) impact of n -doping concentration on electrical response for lower p doping concentration, (d) impact of p doping concentration on electrical response, (e) impact of p zone thickness on electrical response, (f) influence of temperature on electrical response.

62 creation energy of an electron/hole pair. Experimental determination procedures of C_r with high-energy beams led to
 63 values around 2.4 times the SiC bandgap [17], however, for our simulations we have set it at the SiC bandgap value
 64 (3.21 eV), since we are considering radiation-matter interaction of weak energies in a cooled semiconductor, that will
 65 annihilate the phonons contribution. Although this approach can slightly overestimate the absolute number of generated
 66 electron-hole pairs, it will not change the fundamental conclusions on the following simulations, since we will perform
 67 relative optimization of electrical response on several varying parameters of the diode.

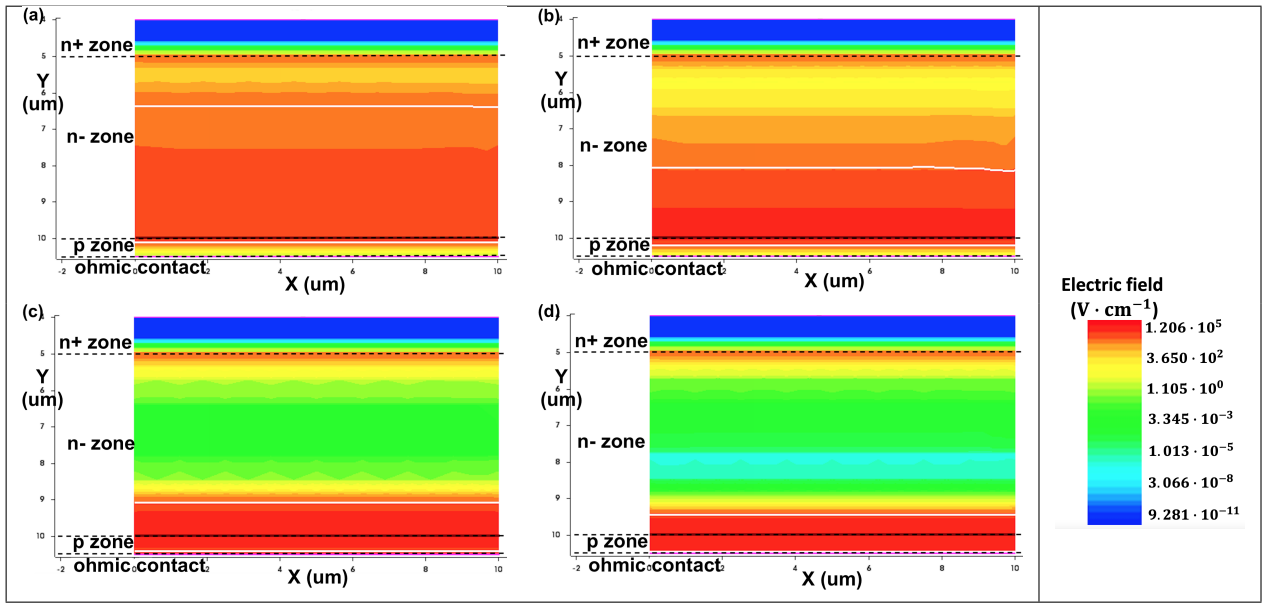


Figure 3: Electrical field profiles in SiC (in $\text{V} \cdot \text{cm}^{-1}$) associated to the plots of Figure 2c (p zone thickness 500 nm, p doping concentration $1 \cdot 10^{16} \text{ atm} \cdot \text{cm}^{-3}$, 5V reverse bias): (a), (b), (c) and (d) respectively corresponds to $5 \cdot 10^{14}$, $1 \cdot 10^{15}$, $5 \cdot 10^{15}$, $1 \cdot 10^{16} \text{ atm} \cdot \text{cm}^{-3}$ $n-$ doping concentration. White lines correspond to depletion region limits.

Then, from the electron-hole generation rate, we have implemented a finite-element modelling, using Sentaurus code, of the electrical response of a SiC-based PIN diode with Al coating, submitted to a tritiated sample irradiation (diode structure presented on Figure 2a). Using the Incomplete Ionization Model for the acceptor doping, we have studied the impact on electrical response of three diode parameters, namely p zone thickness, p doping concentration, $n-$ doping concentration, varying on respective $[100 \text{ nm}, 500 \text{ nm}]$, $[5 \cdot 10^{14} \text{ atm} \cdot \text{cm}^{-3}, 1 \cdot 10^{19} \text{ atm} \cdot \text{cm}^{-3}]$, $[5 \cdot 10^{14} \text{ atm} \cdot \text{cm}^{-3}, 1 \cdot 10^{16} \text{ atm} \cdot \text{cm}^{-3}]$ domains (full data in Supplementary Material). We have also verified that 1D-defects have negligible impact on electrical response (see Supplementary Material).

In a first step, we have computed the electrical response for four values of $n-$ doping concentrations (Fig. 2b and 2c). One can see that $n-$ doping concentration has a weak impact for high concentrations in p zone (Fig. 2b), and a strong impact for lower concentrations in p zone (Fig. 2c). In the low p concentration case (Fig. 2c), the dispersion in electrical response with $n-$ concentrations is due to the trade-off between depletion region and beta-induced electron-hole generation. To illustrate that point, we have reproduced on Figure 3 the electric field profiles associated to the four plots of Figure 2c: one can clearly see a more intense electric field at the $p/n-$ junction (peak of electric field, see associated plots in Supplementary Material) when doping concentration in $n-$ zone is equivalent to the one of p zone.

In a second step, we have evaluated the impact of doping concentrations in p zone, by plotting the electrical response for six p doping concentration values (Fig. 2d). The procedure has revealed a better electrical response with the decreasing of doping concentration in p zone. Consequently, we will preferentially employ a doping concentration in p diode lower than $2 \cdot 10^{15} \text{ atm} \cdot \text{cm}^{-3}$.

In a third step, we have estimated the impact of p zone thickness, by plotting the electrical response for five thickness values of p zone (Fig. 2e). The path revealed that the electrical response increases when p zone thickness decreases. Our technological objective will thus be a p zone thickness between 100 and 200 nm.

Finally, we have estimated on Fig. 2f the impact of temperature variation on electrical response, using 500 nm thick p zone and $2 \cdot 10^{15} \text{ atm} \cdot \text{cm}^{-3}$ (resp. $5 \cdot 10^{14} \text{ atm} \cdot \text{cm}^{-3}$) p (resp. $n-$) doping concentration. The path revealed a slight increase of the electrical response when temperature decreases, enhancing the interest to cool down the diode in order to maximize its detection efficiency.

These finite elements simulations have given some important information for the future diode conception step. Starting from a given SiC substrate with $n+$ doping at $5 \cdot 10^{19} \text{ atm} \cdot \text{cm}^{-3}$, we will first grow a $5 \mu\text{m}$ - thick SiC layer by epitaxy with implantation of $n-$ dopants at $5 \cdot 10^{14} \text{ atm} \cdot \text{cm}^{-3}$. On this $n-$ zone, we will then grow a SiC p zone at $1 \cdot 10^{16} \text{ atm} \cdot \text{cm}^{-3}$ concentration, that will not exceed 200 nm in thickness. After adding the thin ohmic contact made

of low-density metal, we will then couple the diode to a liquid nitrogen cooling mechanism in order to maximize its electrical response.

To conclude, our preliminary Monte-Carlo investigations have enhanced the necessity to work under vacuum, employ very thin coatings layers of low-density materials, and use the upstream surface part of SiC in order to optimize the tritium betavoltaic detection process. The deposited energies computed in Monte-Carlo have then been used to implement finite elements calculations, that led to an optimal design for the PIN diode represented on Fig. 2a, maximizing the electrical response: (i) n -doping concentration of $5 \cdot 10^{14} \text{ atm} \cdot \text{cm}^{-3}$, (ii) maximal doping concentration in p doping equal to $1 \cdot 10^{16} \text{ atm} \cdot \text{cm}^{-3}$, (iii) maximal thickness of p zone equal to 200 nm. Temperature-dependent simulations revealed the interest to cool down the diode in order to optimize its electrical response.

Acknowledgments

This work received support from the french government under the France 2030 investment plan, as part of the Initiative d'Excellence d'Aix-Marseille Université - A*MIDEX.

Data Availability Statement

The data supporting the findings of this study are available upon request.

CRedit authorship contribution statement

Paul Eyméoud: Conceptualization, Methodology, Software, Investigation, Writing - Original Draft, Writing - Review and Editing. **Stéphane Biondo:** Conceptualization, Methodology, Software, Investigation. **Vanessa Vervisch:** Validation, Supervision. **Laurent Ottaviani:** Validation. **Nadia Grillet:** Funding Acquisition, Validation. **Luc Roussel:** Validation. **Karine Coulié:** Software, Validation. **Olivier Palais:** Validation. **Julien Darréon:** Validation. **Wilfried Vervisch:** Validation, Supervision.

References

- [1] B. Nie, S. Fang, M. Jiang, L. Wang, M. Ni, J. Zheng, Z. Yang, and F. Li *Renewable and Sustainable Energy Reviews*, vol. 135, p. 110188, 2021. <https://doi.org/10.1016/j.rser.2020.110188>.
- [2] A. J. Parker, M. D. Aspinall, C. Boxall, F. D. Cave, and M. J. Joyce *Progress in Nuclear Energy*, vol. 162, p. 104733, 2023. <https://doi.org/10.1016/j.pnucene.2023.104733>.
- [3] P. Fichet, A. Bultel, S. Markelj, and C. Moreno, "Review of the different techniques to analyze tritium," technical report, CEA, 2018.
- [4] W. R. Wampler and B. L. Doyle *Nuclear Instruments and Methods in Physics Research A*, vol. 349, p. 473, 1994. [https://doi.org/10.1016/0168-9002\(94\)91213-0](https://doi.org/10.1016/0168-9002(94)91213-0).
- [5] S. I. Maximenko, J. E. Moore, C. A. Affouda, and P. P. Jenkins *Scientific Reports*, vol. 9, p. 10892, 2019. <https://doi.org/10.1038/s41598-019-47371-6>.
- [6] M. Culcer, M. Iliescu, M. Curuia, A. Enache, I. Stefanescu, C. Ducu, and V. Malinovschi *Progress of Cryogenics and Isotopes Separation*, vol. 7, 2004. <https://www.energ-en.ro/pages/article/359>.
- [7] B. A. VanDevender, L. I. Bodine, A. W. Myers, J. F. Amsbaugh, M. A. Howe, M. L. Leber, R. G. H. Robertson, K. Tolich, T. D. V. Wechel, and B. L. Wall *Nuclear Instruments and Methods in Physics Research A*, vol. 673, p. 46, 2012. <https://doi.org/10.1016/j.nima.2012.01.033>.
- [8] B. Liu, K. P. Chen, N. P. Kherani, and S. Zukotynski *Applied Physics Letters*, vol. 95, p. 233112, 2009. <https://doi.org/10.1063/1.3272105>.
- [9] A. M. Barnett, J. E. Lees, and D. J. Bassford *JINST*, vol. 7, p. 09012, 2012. <https://iopscience.iop.org/article/10.1088/1748-0221/7/09/P09012>.
- [10] P. Cabauy, L. C. Olsen, and N. Pan. U.S. Patent No. US9887018B2, Feb. 6 2018. <https://patents.google.com/patent/US9887018B2/en>.
- [11] J. F. Briesmeister, "Mcnp – a general monte-carlo n-particle transport code," technical report, Los Alamos National Laboratory, 1993. <https://api.semanticscholar.org/CorpusID:123810257>.
- [12] Synopsys. Sentaurus Device Manual, Santa Clara, 2010. <https://www.synopsys.com/manufacturing/tcad/device-simulation/sentaurus-device.html>.
- [13] P. Eyméoud, S. Biondo, V. Vervisch, N. Grillet, and L. Ottaviani *EPJ Web of Conferences*, vol. 288, p. 10020, 2023. <https://doi.org/10.1051/epjconf/202328810020>.
- [14] M. Litz, "Monte-carlo evaluation of tritium beta spectrum energy deposition in gallium nitride (gan) direct energy conversion devices," 2014. <https://apps.dtic.mil/sti/pdfs/ADA609481.pdf>.
- [15] M. Hara, T. Shimura, K. Aoki, M. Matuyama, T. Aso, and M. Rollig *Fusion Engineering and Design*, vol. 172, p. 112814, 2021. <https://doi.org/10.1016/j.fusengdes.2021.112814>.
- [16] F. M. Frankle, "Katrin: an experiment to determine the neutrino mass," 2011. Proceedings of the DFT-2011 Conference, Providence, RI, <https://arxiv.org/pdf/1110.0087.pdf>.
- [17] A. Gsponer, M. Knopf, P. Gaggl, J. Burin, S. Waid, and T. Bergauer *Nuclear Instruments and Methods in Physics Research A*, vol. 1064, p. 169412, 2024. <https://doi.org/10.1016/j.nima.2024.169412>.